



CD276 regulates the immune escape of esophageal squamous cell carcinoma through CXCL1–CXCR2 induced NETs

Gan Xiong,¹ Zhi Chen,¹ Qianwen Liu,² Fang Peng,³ Caihua Zhang,¹ Maosheng Cheng,¹ Rongsong Ling,⁴ Shuang Chen,¹ Yu Liang,¹ Demeng Chen ¹, Qimin Zhou ⁵

To cite: Xiong G, Chen Z, Liu Q, *et al.* CD276 regulates the immune escape of esophageal squamous cell carcinoma through CXCL1–CXCR2 induced NETs. *Journal for ImmunoTherapy of Cancer* 2024;**12**:e008662. doi:10.1136/jitc-2023-008662

► Additional supplemental material is published online only. To view, please visit the journal online (<https://doi.org/10.1136/jitc-2023-008662>).

GX, ZC, QL, FP and CZ contributed equally.

Accepted 29 April 2024

ABSTRACT

Background CD276 (B7-H3), a pivotal immune checkpoint, facilitates tumorigenicity, invasiveness, and metastasis by escaping immune surveillance in a variety of tumors; however, the underlying mechanisms facilitating immune escape in esophageal squamous cell carcinoma (ESCC) remain enigmatic.

Methods We investigated the expression of CD276 in ESCC tissues from patients by using immunohistochemistry (IHC) assays. In vivo, we established a 4-nitroquinoline 1-oxide (4NQO)-induced CD276 knockout (CD276^{WKO}) and K14cre; CD276 conditional knockout (CD276^{CKO}) mouse model of ESCC to study the functional role of CD276 in ESCC. Furthermore, we used the 4NQO-induced mouse model to evaluate the effects of anti-CXCL1 antibodies, anti-Ly6G antibodies, anti-NK1.1 antibodies, and GSK484 inhibitors on tumor growth. Moreover, IHC, flow cytometry, and immunofluorescence techniques were employed to measure immune cell proportions in ESCC. In addition, we conducted single-cell RNA sequencing analysis to examine the alterations in tumor microenvironment following CD276 depletion.

Results In this study, we elucidate that CD276 is markedly upregulated in ESCC, correlating with poor prognosis. In vivo, our results indicate that depletion of CD276 inhibits tumorigenesis and progression of ESCC. Furthermore, conditional knockout of CD276 in epithelial cells engenders a significant downregulation of CXCL1, consequently reducing the formation of neutrophil extracellular trap networks (NETs) via the CXCL1–CXCR2 signaling axis, while simultaneously augmenting natural killer (NK) cells. In addition, overexpression of CD276 promotes tumorigenesis via increasing NETs' formation and reducing NK cells in vivo.

Conclusions This study successfully elucidates the functional role of CD276 in ESCC. Our comprehensive analysis uncovers the significant role of CD276 in modulating immune surveillance mechanisms in ESCC, thereby suggesting that targeting CD276 might serve as a potential therapeutic approach for ESCC treatment.

INTRODUCTION

Esophageal cancer (EC) is the ninth common cancer and the sixth leading cause of cancer-related mortality.^{1,2} In 2020, EC

WHAT IS ALREADY KNOWN ON THIS TOPIC

⇒ The immune checkpoint inhibitor CD276 has been used in the treatment of various tumors. However, additional efforts should be made to explore the mechanisms through which CD276 mediates immune evasion in esophageal squamous cell carcinoma (ESCC).

WHAT THIS STUDY ADDS

⇒ We identified that CD276 promoted tumor development by facilitating tumor-neutrophil interactions and inducing the formation of neutrophil extracellular trap networks (NETs) via the CXCL1/CXCR2 axis. Therefore, targeting neutrophils and NETs can augment the number of natural killer cells, thereby inhibiting tumor progression.

HOW THIS STUDY MIGHT AFFECT RESEARCH, PRACTICE, OR POLICY

⇒ Our findings reveal a significant role of CD276 as a biomarker and potential therapeutic target for ESCC treatment. Furthermore, our data presents a promising strategy for enhancing the management of immunotherapy in ESCC.

was responsible for the deaths of more than 500 000 individuals worldwide.^{1,3} Traditionally, EC has been classified into esophageal squamous cell carcinoma (ESCC) and esophageal adenocarcinoma (EAC) based on pathologic diagnosis. ESCC represents the predominant subtype of EC, comprising 80% of all EC cases, and can arise anywhere along the esophagus.⁴ The progression of ESCC is associated with various risk factors, including tobacco, alcohol, heat injuries, and micronutrient deficiencies.² Nowadays, the therapeutic approaches for ESCC predominantly encompass surgical excision, supplemented with radiotherapy and chemotherapy. However, the prognosis for patients remains dismal, with low 5-year survival rate, frequent local recurrence, and rapid lymph node metastasis.^{5,6} Therefore, it is an urgent



© Author(s) (or their employer(s)) 2024. Re-use permitted under CC BY-NC. No commercial re-use. See rights and permissions. Published by BMJ.

For numbered affiliations see end of article.

Correspondence to

Dr Qimin Zhou;
qimin.zhou@sjtu.edu.cn

Dr Demeng Chen;
chendm29@mail.sysu.edu.cn

need to find a new therapeutic target and enhance the treatment efficacy for ESCC.

In recent years, immunotherapy has been employed in the treatment of various tumors, including melanoma, lung cancer, head and neck squamous cell carcinoma, gastric cancer, ovarian cancer, and ESCC.^{7–9} Immune checkpoint inhibitors (ICIs), such as anti-cytotoxic T-lymphocyte-associated antigen 4 (anti-CTLA-4) and anti-programmed cell death protein 1 (anti-PD-1), have been considered as promising therapeutic targets in cancer treatment.¹⁰ In several clinical studies focused on immunotherapy, ICIs have been recognized for enhancing the survival rates of patients afflicted with ESCC.^{11–12} However, multiple clinical trials demonstrated that many patients with ESCC experienced no therapeutic advantages from immunotherapy,^{13–15} and only 10%–20% patients with ESCC exhibited a response to ICI monotherapy.¹⁶ Therefore, a profound exploration into the mechanisms of immunotherapy resistance and the identification of potential biomarkers for those patients with ESCC are imperative. B7-H3 (also known as CD276) is an immune checkpoint molecule prominently expressed in various tumor tissues, including triple-negative breast cancer, non-small cell lung cancer, and head and neck squamous cell cancers but rarely expressed in normal tissues.^{17–19} The mechanisms through which CD276 mediates tumor immune evasion are multifaceted, including the reduction of CD8⁺ T cells and natural killer (NK) cells and suppression of T helper type 1-mediated immune responses.^{20–21} However, the mechanism by which CD276 modulates immune escape in ESCC remains elusive, lacking in-depth mechanistic study.

In this study, we identified that CD276 was highly expressed in ESCC and promotes tumorigenesis. Mechanistically, overexpression of CD276 promoted tumorigenesis through inducing the formation of neutrophil extracellular trap networks (NETs) and reducing the number of NK cells. Importantly, inhibition of CD276 markedly reduced the expression of CXCL1, diminished the formation of NETs through the CXCL1–CXCR2 axis, and increased NK cells.

RESULTS

Overexpression of CD276 is associated with worse survival of patients with ESCC

We performed immunohistochemical (IHC) staining to detect the CD276 expression in ESCC via two independent cohorts. The Sun Yat-sen University Cancer Center (SYSUCC) cohort, including 297 patients, was evaluated alongside The First Affiliated Hospital Sun Yat-sen University (FAH-SYSU) cohort that comprised 143 patients. Clinical characteristics of the patients from both cohorts are shown in online supplemental tables S1 and S2. IHC staining results showed that CD276 was predominantly expressed on the membrane of tumor cells (figure 1A,G). In the SYSUCC cohort, CD276 expression in para-tumor tissues was significantly lower than that in ESCC tissues

(figure 1B). In both cohorts, the positive ratio of CD276 expression gradually increased from grade I and II to grade III ESCC (figure 1C,H), and the expression of CD276 was significantly elevated in patients with ESCC with late stages (stage3+4) compared with whom with early stages (stage1+2) (figure 1D,I). These findings indicated that CD276 protein was stepwisely upregulated during the malignant transformation of ESCC. Of note, CD276 expression in the recurrent group was significantly higher than the primary group in the SYSUCC cohort (figure 1E). At the same time, we found that patients with better first-line therapy outcomes displayed lower CD276 expression in FAH-SYSU cohort (figure 1J). In addition, the impact of CD276 on the survival of patients with ESCC was also analyzed. Patients with ESCC with high CD276 expression have worse overall survival (OS) than those with low CD276 expression (figure 1F,K). It is noteworthy that among patients with grade II and III ESCC, those with high CD276 expression exhibit worse OS, whereas there is a comparable OS among patients with grade I ESCC (online supplemental figure S1A–F). The median progression-free survival at first-line therapy was also shorter in patients with high versus low CD276 expression in FAH-SYSU cohort (figure 1L). Taken together, CD276 was highly expressed in ESCC and associated with worse survival.

CD276 whole body knockout inhibits ESCC tumorigenesis in vivo

To explore the role of CD276 in ESCC, we generated CD276 whole body knockout (CD276-wKO) mice (figure 2A). Consistent with the previous study,²¹ CD276-wKO mice were born at the expected Mendelian ratios and developed normally. We then used 4-nitroquinoline 1-oxide (4NQO) to induce ESCC in CD276-wKO mice and their control littermates (CD276-CTL). Knockout of CD276 was validated by immunofluorescence staining, which showed that CD276 protein expression was detected in wild type (WT) mice but absent in CD276-wKO mice (figure 2B). In comparison to the control group, which exhibited thick and palpable protuberances in most of the cases, the esophageal tissues in CD276-wKO mice appeared less severe on gross examination (figure 2C). In addition, CD276-wKO mice showed smaller size and lower number of esophageal lesions compared with control mice (figure 2D,E). Global depletion of CD276 greatly reduced the formation of high-grade ESCC (figure 2F,G). Moreover, we found decrease of cell proliferation (Ki67) and increase of cell apoptosis (active-Caspase3) in tumor area of CD276-wKO mice compared with that of the WT mice (figure 2H–K). Murine CD276 is known as a negative regulator of T cells and NK cells.^{20–22} Hence, we characterized the infiltration of CD4⁺, CD8⁺ T cells, and NK cells in ESCC after CD276 depletion. WT and CD276-wKO mice have comparable numbers of intratumoral CD4⁺ T cells (figure 2L,M). However, the intratumoral infiltration of CD8⁺ T cells increased significantly in CD276-wKO compared with WT mice (figure 2N,O).

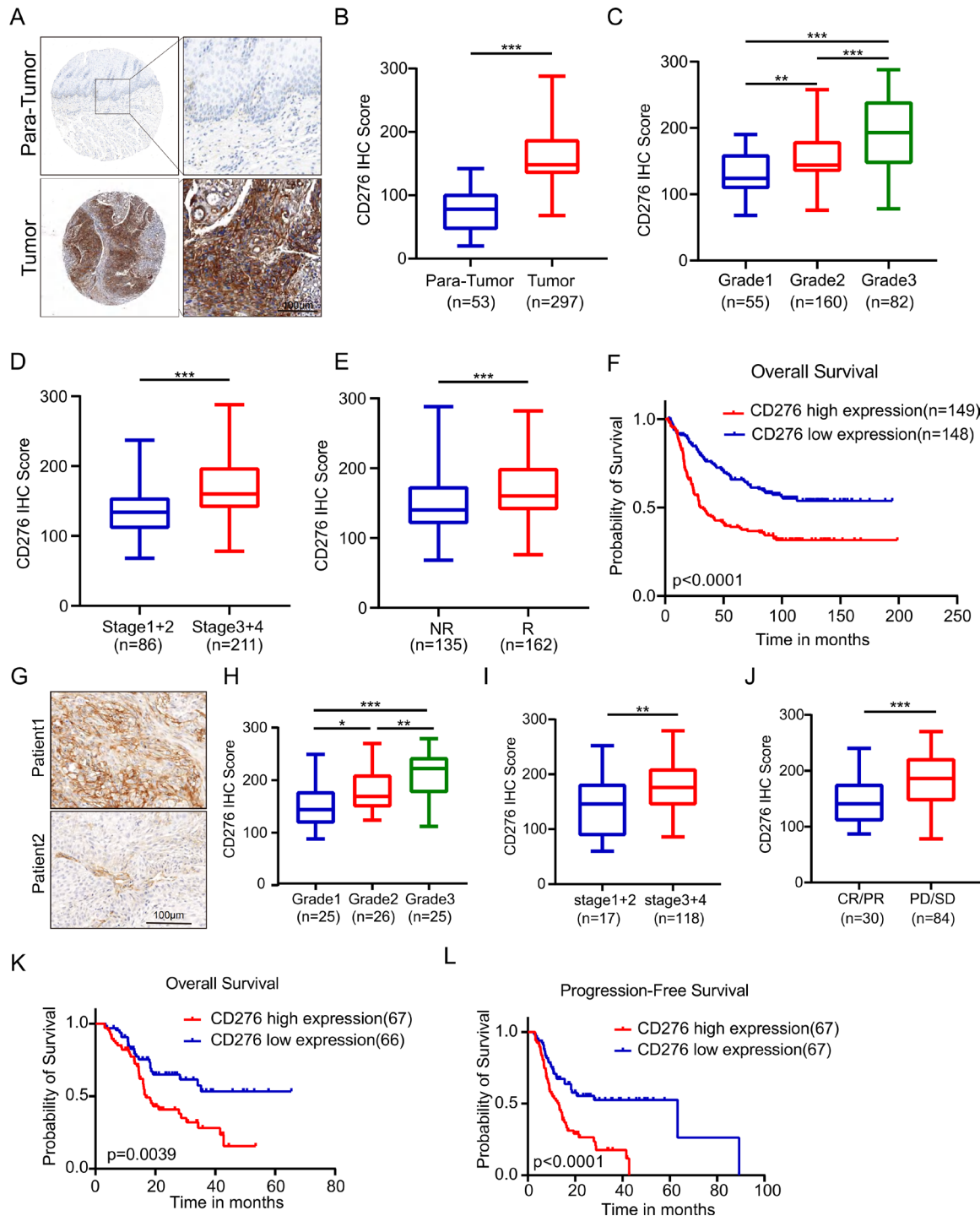


Figure 1 CD276 upregulated expression is associated with clinical parameters and overall survival in patients with ESCC. (A) Representative IHC staining images for CD276 expression in para-tumor and ESCC chips in the SYSUCC patients' cohort. Scale bar, 100 μ m. (B) Statistical analysis of CD276 IHC scores from para-tumor (n=53) and ESCC tissues (n=297) in the SYSUCC patients' cohort. (C) CD276 IHC score representation in the different grades of ESCC in the SYSUCC patients' cohort. (D) CD276 IHC score representation in the recurrence and non-recurrence tumors of ESCC in the SYSUCC patients' cohort. (E) CD276 IHC score representation in the recurrence and non-recurrence tumors of ESCC in the SYSUCC patients' cohort. (F) Kaplan-Meier survival curves stratified by CD276 IHC score based on the median in ESCC tissues from the SYSUCC patients' cohort. (G) Representative IHC staining images for high (upper) and low (lower) CD276 expression of ESCC tissues in the FAH-SYSU patients' cohort. Scale bar, 100 μ m. (H, I) CD276 IHC score representation in the different grades (H) and stages (I) of ESCC in the FAH-SYSU patients' cohort. (J) CD276 IHC score representation in the complete remission/partial remission (PR/CR) and progressive disease/stable disease (PD/SD) group of ESCC in the FAH-SYSU patients' cohort. (K, L) Overall survival curve (K) and Kaplan-Meier progression-free survival (L) stratified by CD276 IHC score based on the median in ESCC tissues from the FAH-SYSU patients' cohort. ESCC, esophageal squamous cell carcinoma; FAH-SYSU, The First Affiliated Hospital Sun Yat-sen University; IHC, immunohistochemistry; SYSUCC, Sun Yat-sen University Cancer Center.

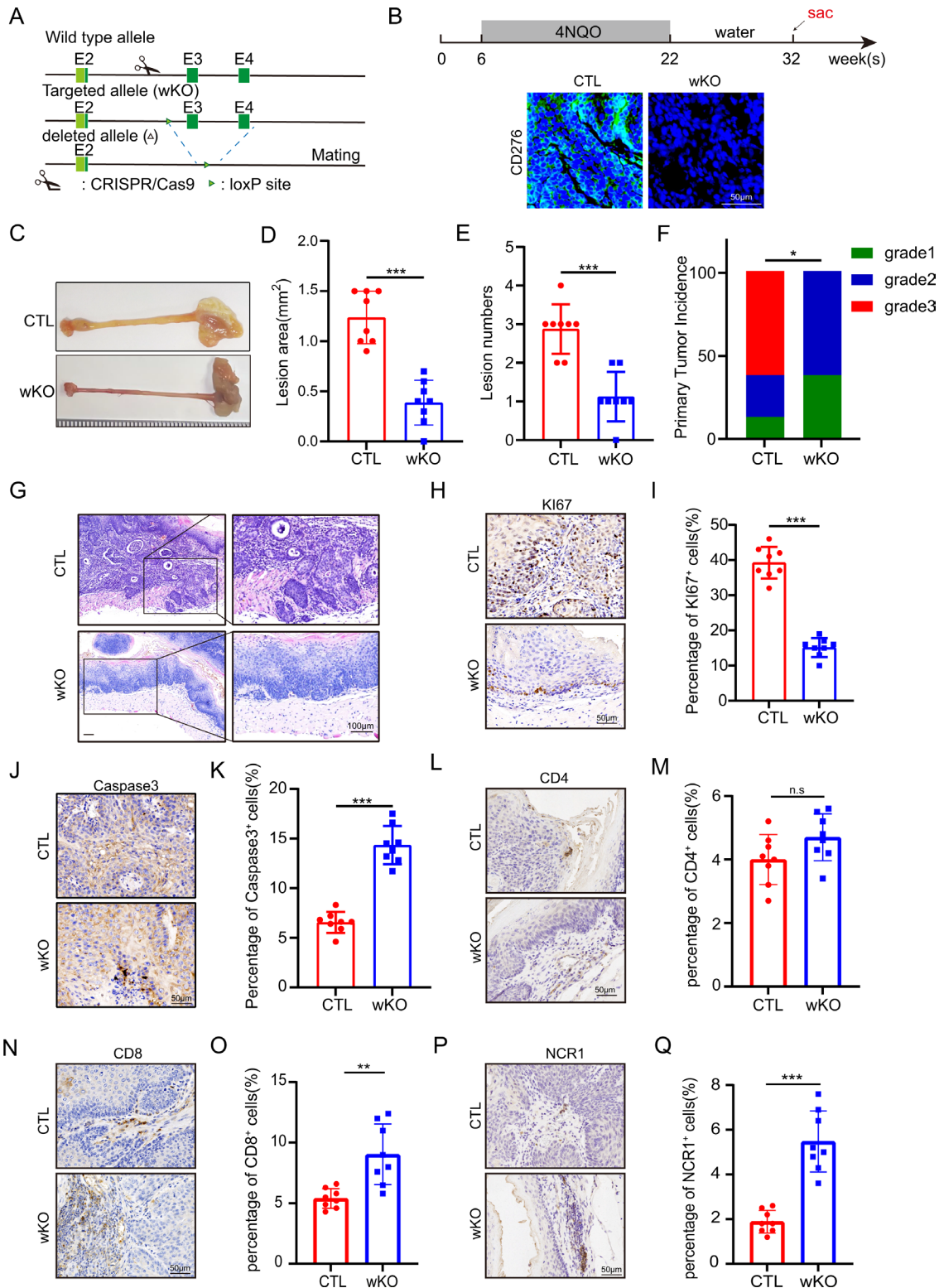


Figure 2 CD276 whole body knockout and blockade inhibits tumorigenesis. (A) Construction of CD276-whole body knockout (wKO) mice. (B) Experimental strategy for the 4NQO-induced ESCC mice model and immunofluorescence images of CD276 in wild-type (WT) and wKO group. Scale bar, 50 μm. (C) Representative esophagi image from 4NQO-induced WT mice and mice with systemic knockdown of CD276 (wKO). The control (CTL) represents the WT group. (D, E) Quantification of lesion area (D) and lesion number (E) of the WT and wKO group. Data are presented as mean±SD (n=8). (F) Quantification of ESCC tumor grade in the WT and wKO group. (G) Representative images of H&E staining in the WT and wKO group. Scale bar, 100 μm. (H–K) Representative images of Ki67 (H) and Caspase3 (J) IHC staining and quantification of percentage of Ki67⁺ (I) and Caspase3⁺ (K) cells in WT and wKO group. Scale bar, 50 μm. (L–Q) Representative images of CD4 (L), CD8 (N), and NCR1 (P) IHC staining and quantification of percentage of CD4⁺ (M), CD8⁺ (O), and NCR1⁺ (Q) cells in WT and wKO group. Scale bar, 50 μm. ESCC, esophageal squamous cell carcinoma; IHC, immunohistochemistry; 4NQO, 4-nitroquinoline 1-oxide.

As shown in [figure 2P,Q](#), the tumor-infiltrated NK cells greatly expanded in CD276-wKO compared with WT mice ($5.5\% \pm 1.4$ in CD276-wKO mice vs $1.9\% \pm 0.5$ in WT mice). Taken together, these findings suggest that whole body knockout CD276 inhibits the ESCC development and progression in vivo.

Epithelial conditional knockout of CD276 suppresses ESCC progression in vivo

CD276 is expressed in both tumor and immune cells.²² We wondered whether the tumorous CD276 is the major driver for ESCC tumorigenesis. To test that, we generated CD276^{fllox} mice and crossed them with K14CreER mice to obtain K14CreER; CD276^{fllox/fllox} mice (CD276-cKO). We then used 4NQO to induce ESCC in cKO and their control littermates (CD276-CTL). We found epithelial depletion of CD276 led to a significant decrease in lesion size and lesion number ([figure 3A–C](#)). In addition, no CD276 expression was detected in the epithelial tissue of CD276-cKO mice ([figure 3D](#)). Similarly, the invasiveness and malignancy of the tumor tissues in the cKO mice were significantly mitigated compared with that in the CD276-CTL mice ([figure 3E,F](#)). Furthermore, Ki67 expression was decreased and active-Caspase3 expression was increased in cKO mice compared with the CD276-CTL mice ([figure 3G–J](#)). To investigate the alterations in the immune microenvironment following the depletion of CD276 in ESCC, we conducted flow cytometry (FCM) to examine changes in immune cell populations. Following the epithelial conditional knockout of CD276 in ESCC, the cKO mice exhibited an increase in intratumoral activated CD8⁺ T cells, whereas neutrophils were reduced. Moreover, the number of CD4⁺ regulatory T cells and macrophages in WT mice was comparable to those in cKO mice (online supplemental figure S2B–M).

Next, to investigate the mechanism of CD276 on the development of ESCC, we resected both control and tumor tissues CD276-cKO for RNA sequencing (RNA-seq). The Kyoto Encyclopedia of Genes and Genomes analysis showed that the PI3K–Akt signaling pathway was significantly downregulated in cKO group compared with WT group ([figure 3K](#)). As shown in [figure 3L–O](#), PI3K and AKT expression were reduced in cKO mice compared with the CD276-CTL mice. These results indicate that CD276 depletion suppresses the progression of murine ESCC and inhibits the effects of the PI3K–Akt signaling pathway in vivo.

CD276 deficiency inhibits tumorigenesis through sharply downregulating CXCL1 expression in vivo

To address the role of tumor cell CD276 on the immune microenvironment of ESCC, we dissected the cancer tissues from one control and two CD276-cKO samples for single-cell RNA sequencing (scRNA-seq). We were able to extract a total of 21 588 high-quality cells (6937 cells in CTL, 7971 cells in cKO-1, and 6680 cells in cKO-2) ([figure 4A](#) and online supplemental figure S3A,B). Based on canonical marker expression, all single cells were

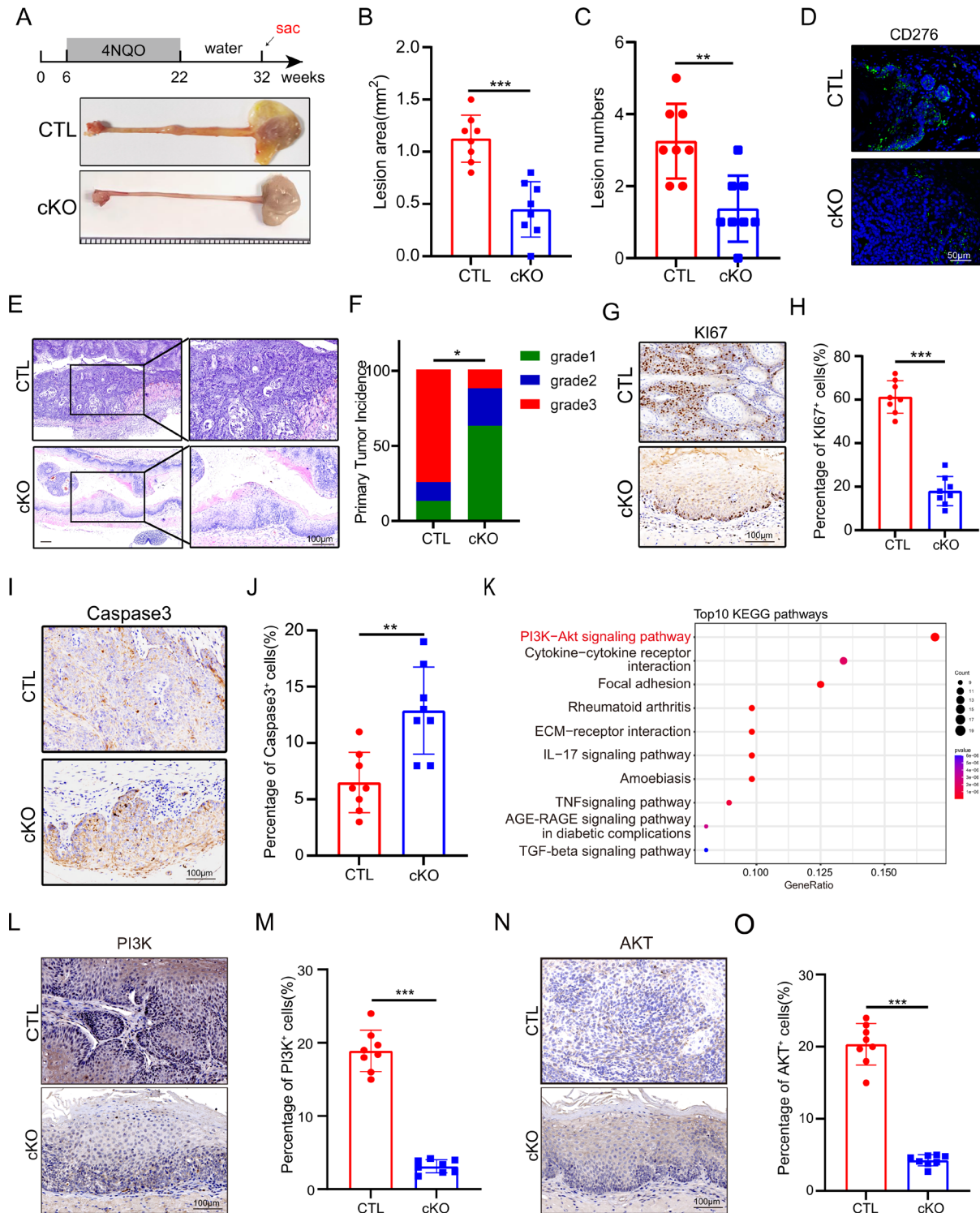
divided into seven major categories, including tumor epithelial cells (Krt5), T cells (Cd3e), M₀M₀DC cells (Cd74), fibroblasts (Col1a1), neutrophils (Csf3r), NK cells (Klrd1), and endothelial cells (Vwf) ([figure 4A,B](#)). It was worth noting that the proportion of neutrophils was lower while the proportion of T cells and NK cells was higher in the CD276-cKO compared with CD276-CTL sample ([figure 4C](#)). We also compared our mouse scRNA-seq dataset with online human ESCC scRNA-seq data comprising 64 ESCC samples.²³ We identified seven major cell populations based on marker expression (online supplemental figure S3C,D). Markedly, we were able to detect B cell population in the human dataset but not in the mouse dataset ([figure 4A](#) and online supplemental figure S3C). More importantly, the cell types detected both in mouse ESCC scRNA-seq and human ESCC scRNA-seq data displayed high similarity in transcriptome (online supplemental figure S3E,F).

To specifically study the effects of CD276 deficiency on epithelial cells, all the epithelial cells were analyzed separately (online supplemental figure S4A). As shown by the volcano plot of the differential expression genes (DEGs) in the scRNA-seq data, Cxcl1 chemokines were most significantly downregulated by CD276 knockdown ([figure 4D](#)). In addition, violin plots also showed that, compared with WT mice, the expression of Cxcl1 chemokine was significantly lower in the cKO mice ([figure 4E](#)). The IHC results further verified the differential expression of CXCL1 between cKO mice and WT mice ([figure 4F,G](#)). Interestingly, the DEGs in the RNA-seq data also demonstrated that Cxcl1 chemokines were markedly downregulated in CD276-cKO group ([figure 4H](#)).

To further analyze the effect of CXCL1 on ESCC, we first used 4NQO to induce ESCC in WT mice, and then half of the ESCC mice were treated with CXCL1 blocking antibody for 1 month, while the other half were treated with anti-IgG antibody. The tumor numbers and sizes were significantly decreased after treatment with CXCL1 blocking antibody ([figure 4I–K](#)). In addition, the proportion of high-grade ESCC was also reduced ([figure 4L](#) and online supplemental figure S4B). Noticeably, Ki67 expression was decreased and active-Caspase3 expression was increased in the mice treated with CXCL1 blocking antibody (online supplemental figure S4C–F). These results indicated that CXCL1 blocking antibody effectively inhibited tumorigenesis of ESCC in mice.

CD276 mediates tumor–neutrophil interactions and induces the formation of NETs via CXCL1/CXCR2 axis

To study whether epithelial cell-specific deficiency of CD276 affects cellular interactions in the tumor microenvironment. Cellchat R package²⁴ was performed to analyze the interactions between tumor epithelial cells and immune cells. The numbers and the intensity of cell interactions were downregulated between tumor cells and T cells/neutrophils in the cKO mice, while compared with the WT group ([figure 5A,B](#)). In addition, among the interactions between tumor epithelial cells and various



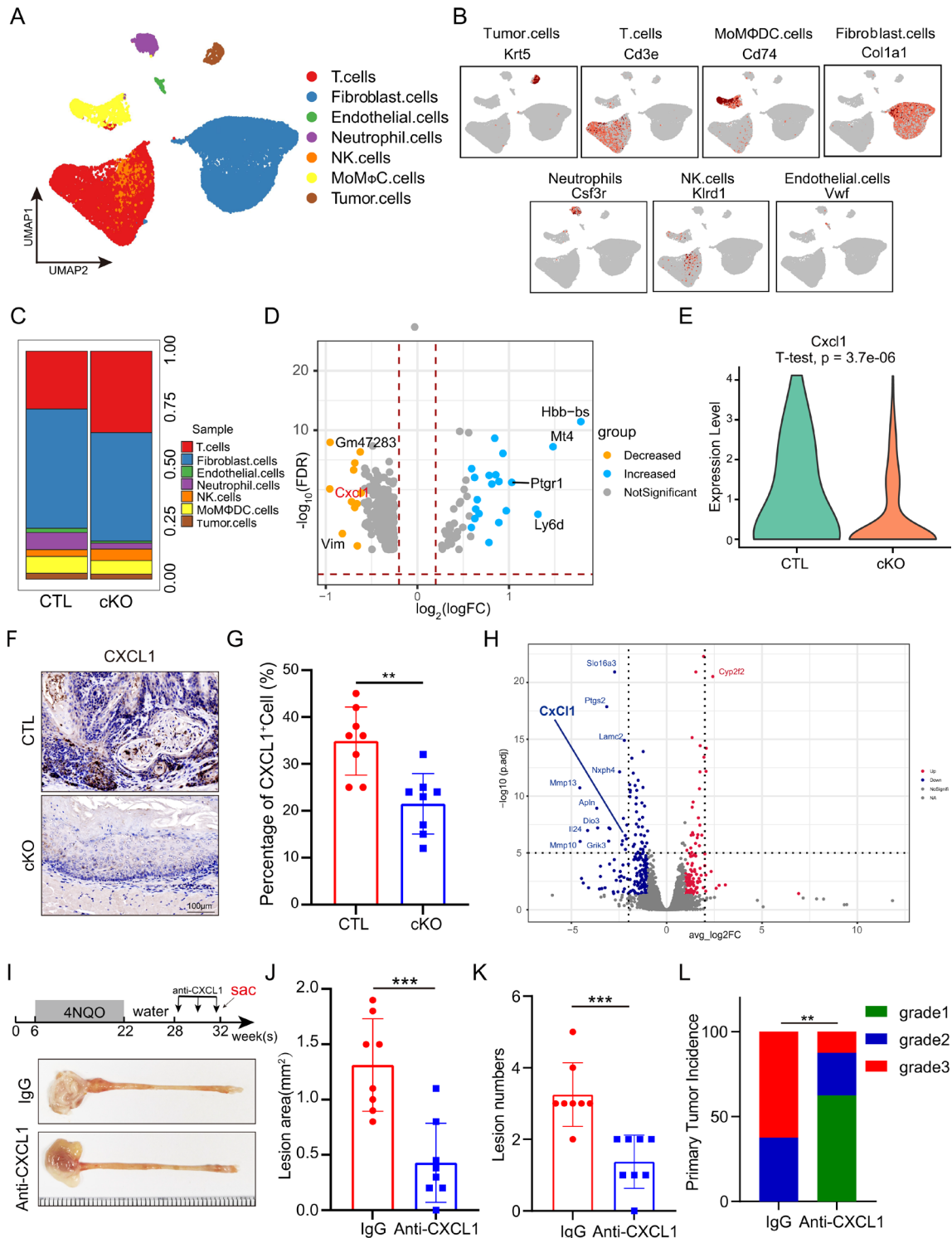


Figure 4 Epithelial-specific CD276 knockdown yielded a significant reduction in CXCL1 expression. (A) UMAP plot displaying identified cell clusters including tumor epithelial cells, fibroblasts, endothelial cells, neutrophils, T cells, NK cells, and MOMΦDC cells. (B) UMAP plot showing the expression of cell-type marker genes. (C) Distribution of the seven major cell clusters in the WT and cKO groups. (D) Volcano plot showing the differential gene in the epithelial cells between WT and cKO groups. (E) Violin plot showing the expression of *Cxcl1* between WT and cKO groups. (F, G) Representative images of CXCL1 (F) IHC staining and quantification of percentage of CXCL1⁺ (G) cells in WT and cKO groups. Scale bar, 100 μm. (H) Volcano plot showing the differentially expressed gene from RNA-seq data between WT and cKO groups. (I) Experimental strategy for the treatment by anti-CXCL1 antibodies and representative esophagi image in mice treated with IgG control (IgG) or anti-CXCL1 antibody group. (J, K) Quantification of lesion area (J) and lesion number (K) of the IgG and anti-CXCL1 group. Data are presented as mean±SD (n=8). (L) Quantification of ESCC tumor grade in the IgG and anti-CXCL1 group. ESCC, esophageal squamous cell carcinoma; FDR, false discovery rate; MOMΦDC, monocyte-macrophage-dendritic cells; IHC, immunohistochemistry; NK, natural killer; UMAP, uniform manifold approximation and projection; WT, wild type.

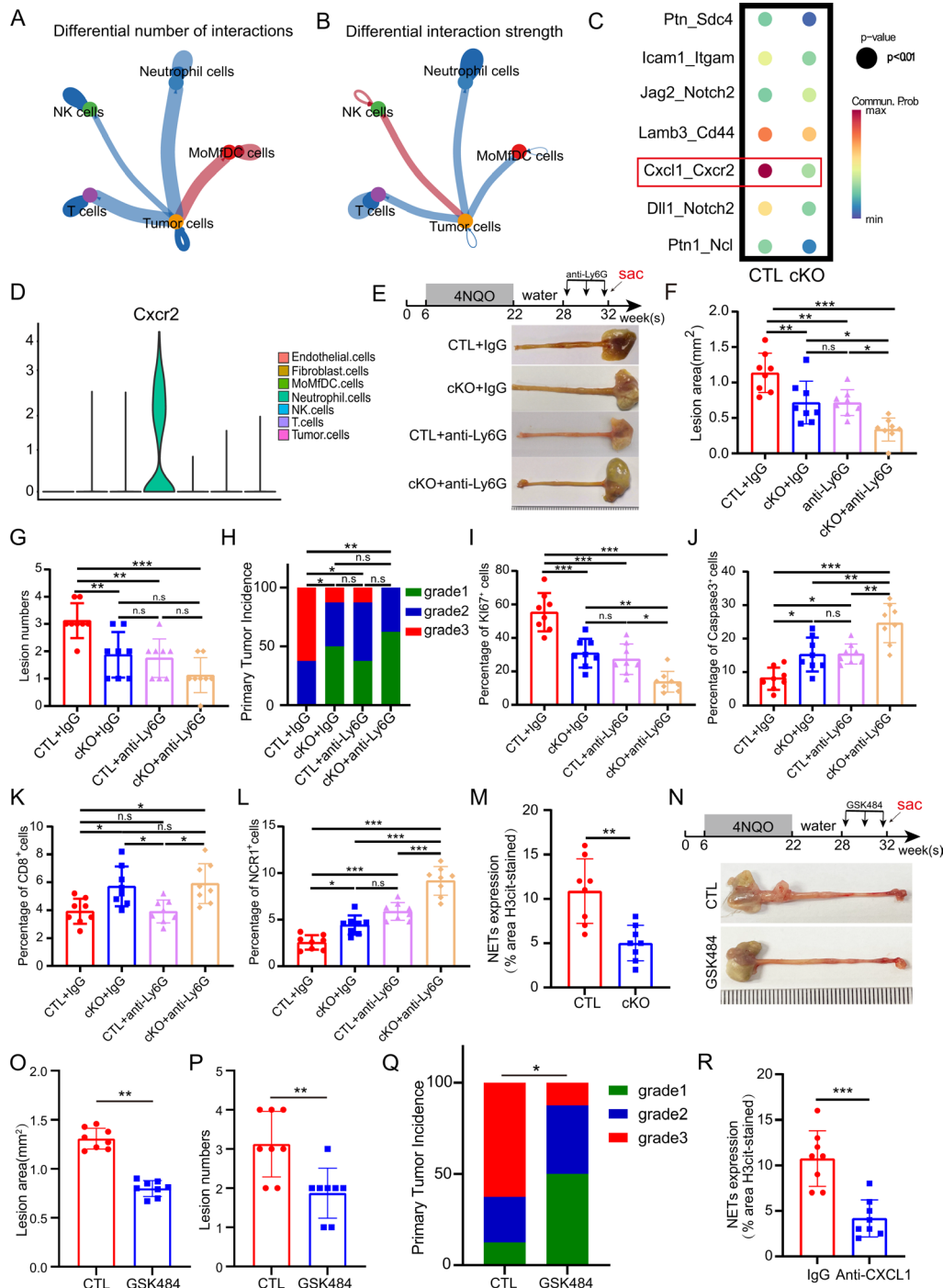


Figure 5 CD276 mediates tumor–neutrophil interactions via CXCL1/CXCR2. (A, B) Circle plots showing the differential interaction number (A) and strength (B) between the tumor cell and immune cell clusters based on CellChat analysis. (C) Dot plot showing the expression of receptor–ligand pairs between tumor cell and immune cell clusters in WT and cKO groups. (D) Violin plot showing the expression of Cxcr2 in different clusters. (E) Experimental strategy for the treatment by anti-Ly6G antibodies and representative esophagi image in mice treated with IgG control (IgG), cKO, anti-Ly6G, or cKO+anti-Ly6G group. (F, G) Quantification of lesion area (F) and lesion number (G) of IgG control (IgG), cKO, anti-Ly6G, or cKO+anti-Ly6G group. Data are presented as mean±SD (n=8). (H) Quantification of ESCC tumor grade in IgG control (IgG), cKO, anti-Ly6G, or cKO+anti-Ly6G group. (I, J) Quantification of percentage of Ki67⁺ (I) and Caspase3⁺ (J) cells in IgG control (IgG), cKO, anti-Ly6G, or cKO+anti-Ly6G group. (K, L) Quantification of percentage of CD8⁺ (K) and NCR1⁺ (L) cells in IgG control (IgG), cKO, anti-Ly6G, or cKO+anti-Ly6G group. (M) Quantification of percentage H3cit⁺ cells of ESCC in control (CTL) and cKO group. (N) Experimental strategy for the treatment by GSK484 inhibitors and representative esophagi image in mice treated with control or GSK484 group. (O, P) Quantification of lesion area (O) and lesion number (P) of the control and GSK484 group. Data are presented as mean±SD (n=8). (Q) Quantification of ESCC tumor grade in the control and GSK484 group. Scale bar, 100 μm. (R) Quantification of percentage H3cit⁺ cells of ESCC in the IgG and anti-CXCL1 group. ESCC, esophageal squamous cell carcinoma; NK, natural killer; 4NQO, 4-nitroquinoline 1-oxide; WT, wild type.

types of immune cells, the Cxcl1–Cxcr2 interactions between tumor cells and neutrophils were the highest intensity (figure 5C). It is noteworthy that the Cxcr2 was mainly expressed in neutrophils, while almost no expression observed in other types of immune cells (figure 5D). Consequently, neutrophil activity was inhibited by employing an anti-Ly6G antibody (online supplemental figure S5A). As shown in figure 5E–G, single depletion of neutrophil activity also affected the numbers and sizes of ESCC and concurrently potentiated the efficacy of the CD276 deficiency.

Subsequently, the pathologic grade of ESCC was also diminished following treatment of the anti-Ly6G antibody (figure 5H and online supplemental figure S5B). Following treatment with the anti-Ly6G antibody, the expression of Ki67 and active-Caspase3 paralleled that observed in the CD276 deficiency mice, and additionally, it augmented the efficacy of the knockout of CD276 (figure 5I,J and online supplemental figure S5C). Interestingly, the numbers of CD8⁺ T cells remained unaltered following treatment with the anti-Ly6G antibody; however, there was a significant augmentation in the number of NK cells after the anti-Ly6G therapy (figure 5K,L, and online supplemental figure S5D). Moreover, FCM analysis was performed to further verify the effect of the anti-Ly6G antibody on T cells and NK cells. In contrast with WT mice, the numbers of CD8⁺ T cells and CD4⁺ T cells remained unaltered in the anti-Ly6G group, while NK cells were elevated, and neutrophils were diminished (online supplemental figure S5E–L). These results indicated that the suppression of neutrophil activity mitigates the progression of ESCC by enhancing NK cell function.

Nonetheless, the mechanism by which neutrophils regulate NK cells remains elusive. Recently, CXCR2 was identified to induce the formation of NETs,^{25–28} which was significantly increased in the cancer progression. By means of fluorescence colocalization, the generation of NETs and neutrophils in cKO mice was significantly lower than that in WT mice (figure 5M and online supplemental figure S6A). To further elucidate the impact of NETs on ESCC, we administered a 1-month treatment with GSK484, a PAD4 inhibitor, to ESCC mice. The results showed that the tumor numbers and sizes were significantly decreased on GSK484 treatment group (figure 5N–P). Particularly, the high grade ESCC was also reduced after treatment with GSK484 inhibitor (figure 5Q and online supplemental figure S6B). As expected, Ki67 expression diminished, whereas Caspase3 expression escalated in tumor cells following treatment with GSK484 inhibitor (online supplemental figure S6C–F). Notably, the NCR1 expression in the cKO mice was significantly higher than in WT mice, and the NETs were generated around NK cells (online supplemental figure S6G–I). Furthermore, the quantity of NETs exhibited a significant reduction following treatment with anti-CXCL1 antibodies (figure 5R and online supplemental figure S6J). To sum up, these results indicate that CD276 orchestrates interactions between tumors and neutrophils, prompting

the formation of NETs via CXCL1/CXCR2 axis. Furthermore, NETs could exert pro-tumor effects by suppressing the activity of NK cells.

Depleting NK cells impedes the efficacy of CD276 deficiency in suppressing the progression of ESCC

To ascertain whether the attenuation of ESCC progression by CD276 depletion is contingent on NK cell activity, NK cells were neutralized with the administration of an anti-NK1.1 antibody. The ablation of NK cells notably reduced the suppressive effect on tumor proliferation observed in CD276-deficient mice, as determined by analyses of tumor count and size (figure 6A–C). Histopathologic examination disclosed that the depletion of NK cells markedly reverted the pathologic grading of ESCC in mice lacking CD276 expression (figure 6D,E). Furthermore, both Ki67 and active-caspase3 expression were also restored to the levels in WT mice in CD276-deficient mice following the administration of the anti-NK1.1 antibody (figure 6F–H). As shown in figure 6I,J, the population of CD8⁺ T cells remained consistent following the administration of the anti-NK1.1 antibody in CD276-deficient mice. As expected, NK cell infiltration was elevated in CD276-deficient mice yet was eliminated with the administration of the anti-NK1.1 treatment (figure 6I–K). Importantly, we explored the association between CD276 expression and NK cells in ESCC samples. IHC assays confirmed that CD276 expression exhibited an inverse correlation with infiltration of NK cells in human ESCC samples (figure 6L). To explore the influence of CD8⁺ T cells in ESCC, the anti-CD8 antibodies were used to explore the functional role of CD8⁺ T cells in ESCC progression following CD276 depletion. After the ablation of CD8⁺ T cells, there was a slight augmentation in tumor numbers and size, resulting in a reduction of the suppressive effect on tumor progression in CD276-deficient mice (online supplemental figure S7A–C). These results revealed that the suppression of ESCC progression by CD276 depletion is primarily mediated through the inhibition of NK cell activity.

CD276 overexpression promotes tumorigenesis in vivo

To further clarify the function of CD276 in ESCC, CD276 overexpression mice (cKI) was constructed. After 4NQO treatment as described above, the esophageal tissues appeared more severe on gross examination in cKI mice compared with the WT mice (figure 7A). In addition, cKI mice developed higher number and larger size of esophageal lesions, respectively, compared with WT mice (figure 7B,C). CD276 overexpression greatly increased the proportion of high-grade ESCC (figure 7D,E). Moreover, we found increased expression of Ki67 and decreased expression of active-Caspase3 in cKI mice compared with WT mice (figure 7F–I). To further verify the effect of CD276 overexpression on neutrophil and NK cells infiltration, we performed FCM and immunofluorescence staining analysis as previously mentioned. Compared with WT mice, the numbers of neutrophils and NETs in the

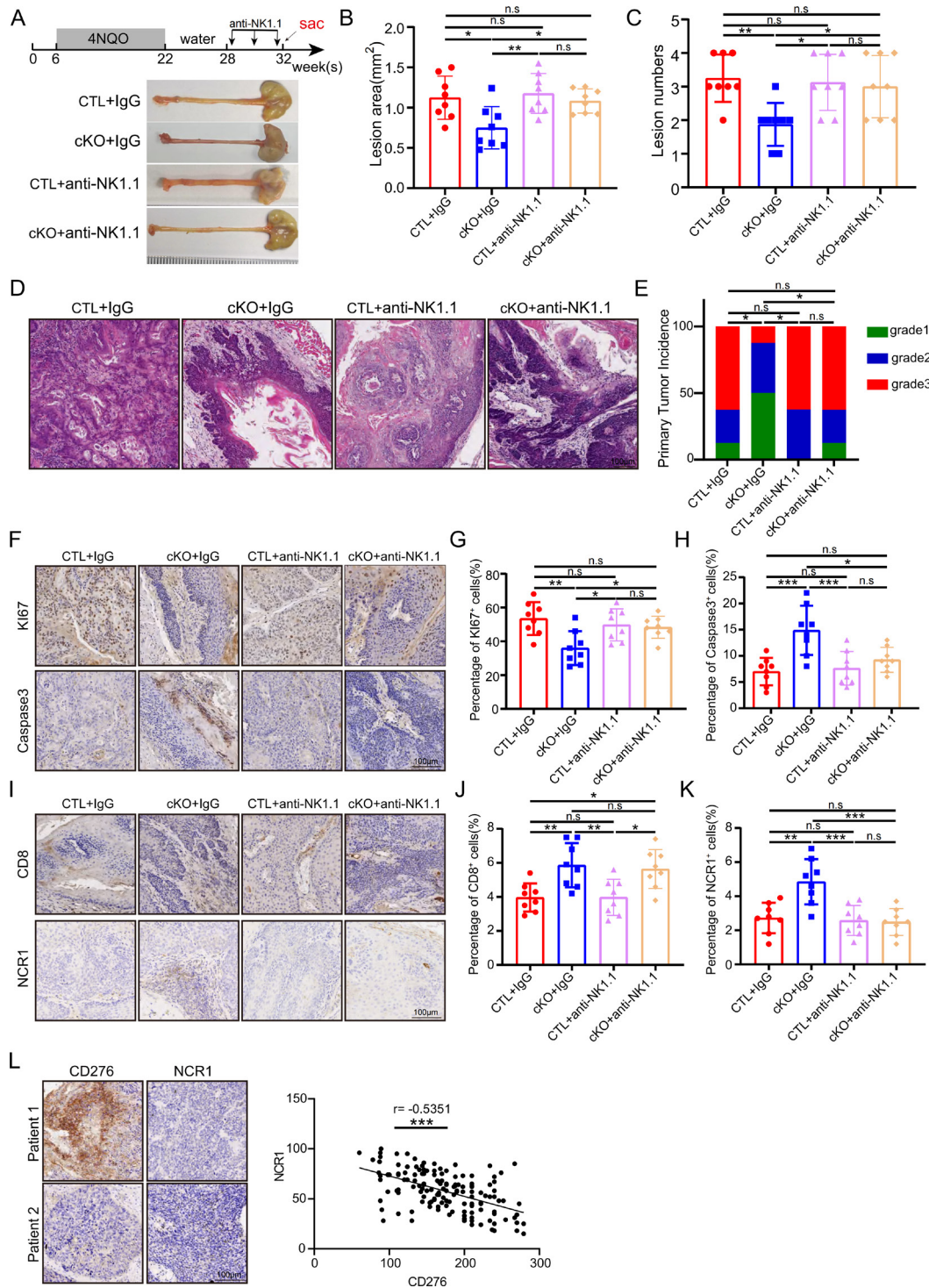


Figure 6 Depleting NK cells impedes the efficacy of CD276 deficiency in suppressing the progression of ESCC. (A) Experimental strategy for the treatment by anti-NK1.1 antibodies and representative esophagi image in mice treated with IgG control (IgG), cKO, anti-NK1.1, or cKO+anti-NK1.1 group. (B, C) Quantification of lesion area (B) and lesion number (C) of IgG control (IgG), cKO, anti-NK1.1, or cKO+anti-NK1.1 group. Data are presented as mean±SD (n=8). (D) Representative images of H&E staining in IgG control (IgG), cKO, anti-NK1.1, or cKO+anti-NK1.1 group. Scale bar, 100µm. (E) Quantification of ESCC tumor grade in IgG control (IgG), cKO, anti-NK1.1, or cKO+anti-NK1.1 group. (F–H) Representative images of Ki67 (F) and Caspase3 (F) IHC staining and quantification of percentage of Ki67⁺ (G) and Caspase3⁺ (H) cells in IgG control (IgG), cKO, anti-NK1.1, or cKO+anti-NK1.1 group. Scale bar, 100µm. (I–K) Representative images of CD8 and NCR1 (I) IHC staining and quantification of percentage of CD8⁺ (J) and NCR1⁺ (K) cells in IgG control (IgG), cKO, anti-NK1.1, or cKO+anti-NK1.1 group. Scale bar, 100µm. (L) Representative images of CD276 and NCR1 IHC staining of ESCC in FAH-SYSU patients' cohort; Scale bar, 100µm (left panel). The correlation between the expression of CD276 and NCR1 was assessed, ***p<0.001 by Pearson (right panel). ESCC, esophageal squamous cell carcinoma; FAH-SYSU, The First Affiliated Hospital Sun Yat-sen University; IHC, immunohistochemistry; NK, natural killer.

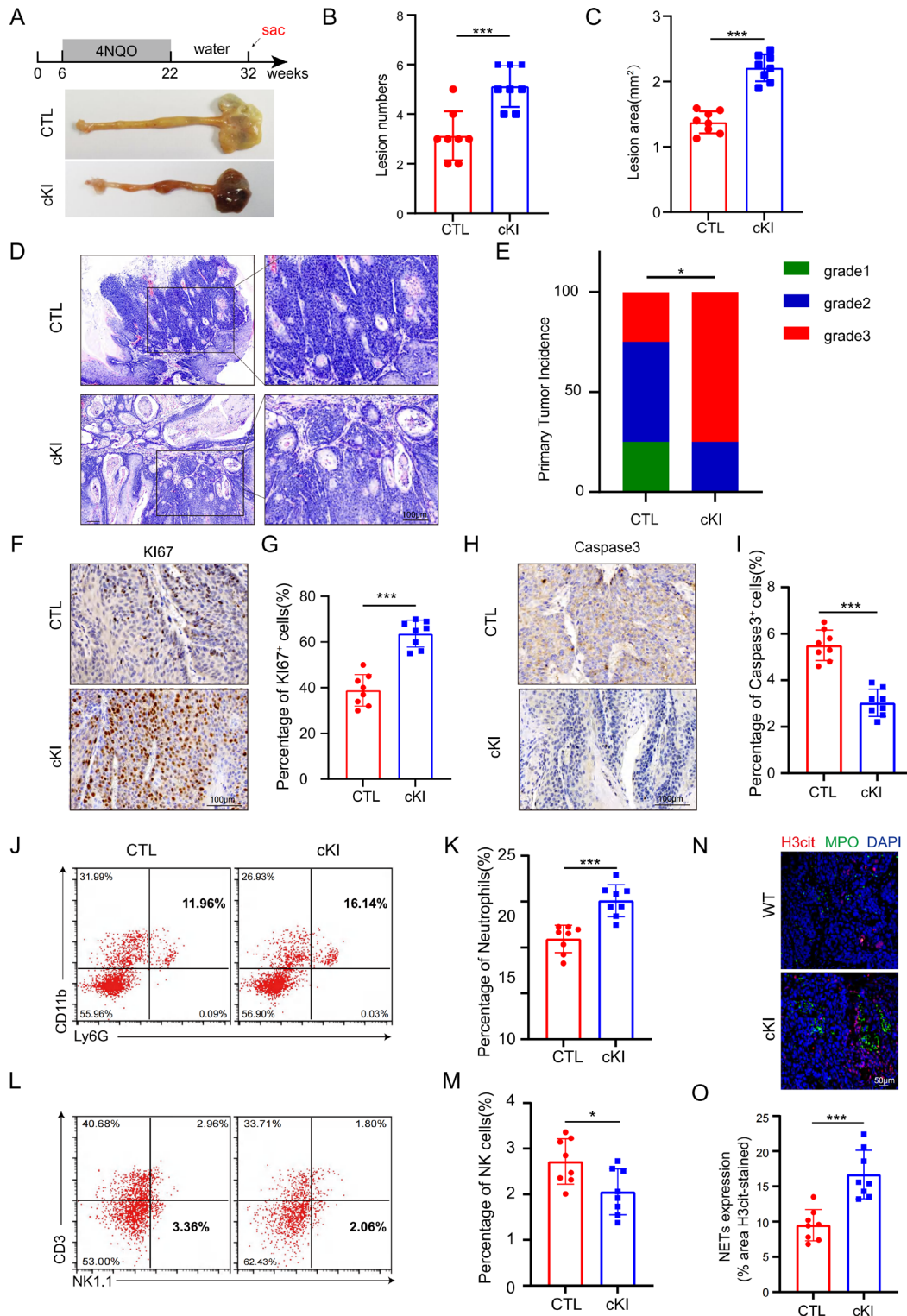


Figure 7 Overexpression of CD276 facilitates tumor progression. (A) Experimental strategy for the 4NQO-induced ESCC mice model and representative esophagi image from 4NQO-induced wild-type mice (WT) and mice with conditional knock-in of CD276 (cKI). (B, C) Quantification of lesion number (B) and lesion area (C) of the WT and cKI group. Data are presented as mean \pm SD (n=8). (D) Representative images of H&E staining in the WT and cKI group. Scale bar, 100 μ m. (E) Quantification of ESCC tumor grade in the WT and cKI group. (F–I) Representative images of Ki67 (F) and Caspase3 (H) IHC staining and quantification of percentage of Ki67⁺ (G) and Caspase3⁺ (I) cells in WT and cKI group. Scale bar, 100 μ m. (J–M) Representative flow cytometry plots indicating neutrophil (J) and NK cells (L) and quantification of the neutrophil (K) and NK cells (M) between WT and cKI group. (N, O) Representative images of H3cit (NETs) and MPO (activated neutrophils) staining (N) and quantification of percentage H3cit⁺ cells (O) of ESCC lesions in WT and cKI group. Nuclei are stained with DAPI (blue). Scale bar, 50 μ m. DAPI, 4',6-diamidino-2-phenylindole; ESCC, esophageal squamous cell carcinoma; IHC, immunohistochemistry; NETs, neutrophil extracellular trap networks; NK, natural killer; 4NQO, 4-nitroquinoline 1-oxide; MPO, myeloperoxidase.

cKI mice were significantly higher (figure 7J, K, N, and O), while NK cells were lower (figure 7L,M).

DISCUSSION

ICIs have been employed in the treatment of various tumors. However, only a minority of individuals benefit from immunotherapy.²⁹ Therefore, the advancement of agents that target supplementary immune checkpoints, costimulatory receptors, and/or coinhibitory receptors, which regulate immune microenvironment, is of paramount importance. The immune checkpoint CD276 is expressed in a variety of tumors and is associated with the progression and prognosis of cancer.^{17–19} In this study, we indicated that CD276 expression levels were significantly elevated in ESCC and significantly correlated with poor prognosis by tumor tissue microarray analysis. We subsequently proceeded to develop an ESCC model in mice with suppression of CD276, facilitating the exploration of CD276 functions within cancer immunity.

The exact function of CD276 in modulating the activity of tumor-infiltrating immune cells and its role in cancer cells is multifaceted, particularly because of the contradictory research that has indicated CD276 act as either a costimulatory or coinhibitory molecule in diverse disease frameworks.^{22–30–32} Additionally, the receptors that bind to B7H3 have not been conclusively determined.³³ Although tumor cells with depletion of CD276 were identified to suppress the progression of tumor depending on CD8⁺ T cells and NK cells.^{19–20} The mechanism by which CD276 deficiency activates the function of immune cells remains elusive. In the current study, our RNA-seq data revealed that CD276 deficiency inhibits tumorigenesis through sharply downregulating CXCL1 expression in vivo. Interestingly, our scRNA-seq data also revealed that conditional knockdown of CD276 in epithelial cells resulted in a marked decrease of CXCL1 expression. Furthermore, the ligand–receptor interaction analysis suggested that CD276 facilitates tumor progression through the CXCL1–CXCR2 axis, with CXCR2 being notably overexpressed in neutrophils. Of note, the connection between CXCR2 and the formation of NETs provides a valuable insight into the complex interplay between chemokines and cancer progression.^{25–28} Our results also indicated that suppression of NETs hampered the progression of ESCC, coupled with a substantial augmentation of NK cells presence within ESCC. This observation may be attributed to the propensity of NETs to impede the cytotoxic functions of both cytotoxic T lymphocytes and NK cells in tumor microenvironment.²⁵

Recently, studies on drug application against CD276 have been reported. The research team led by Gianpietro Doti discovered that targeting CD276 could efficaciously restrain the proliferation of solid neoplasms, including pancreatic ductal adenocarcinoma and ovarian cancer.³⁴ Seaman and colleagues' work contributed to the understanding of CD276 as a cancer-associated marker by showing its overexpression not only in cancer cells

but also in tumor vascular cells and demonstrated that anti-CD276-drug conjugates as promising anticancer reagents.³⁵ In the current study, our results demonstrated that targeting CD276 markedly suppressed the progression of ESCC. The results support the hypothesis that CD276 functions as an immune checkpoint in cancer progression and can be a target to enhance the immune system's ability to fight cancer.

In conclusion, our findings demonstrate that CD276 is markedly overexpressed in ESCC and is associated with an adverse prognosis. Mechanically, depletion of CD276 precipitated a notable diminution in CXCL1 expression, culminating in a diminished infiltration of neutrophils into tumors and a consequent reduction in NETs formation through the CXCL1–CXCR2 axis, concurrently intensifying the infiltration of NK cells to impede tumor progression. In the future, more efforts will be required to develop immunotherapeutic strategies that target CD276 in ESCC.

MATERIALS AND METHODS

Animal assay

K14^{CreER} mice were purchased from The Jackson Laboratory. The Cd276^{wKO/wKO}, Cd276^{cKO/cKO}, and Cd276^{cKI/cKI} mice were purchased from the Biocytogen (Nantong, China). As previously described, mice were treated with 50 µg/mL 4NQO (Sigma, N8141) to induce ESCC formation.³⁶ Briefly, 6-week-old male mice were orally administered with 4NQO dissolved in drinking water for 16 weeks to induce the formation and development of ESCC. Subsequently, the mice were returned to normal water for 10 weeks. For the generation of conditional knockout and knock-in mouse models, tamoxifen (Sigma, T5648-1G) was dissolved in corn oil (Aladdin, C116025-500ml) at a concentration of 10 mg/mL. After 4NQO treatment, tamoxifen was intraperitoneally injected into the mice at a dose of 1 mg/mouse/day for 3 consecutive days to induce the knockout or knock-in of CD276. The ESCC samples were procured for subsequent analytical procedures to assess the impact of CD276 gene ablation or upregulation on the progression of ESCC and its concomitant phenotypic manifestations.

For the blockade treatment, antibodies and inhibitors anti-CXCL1 (CXCL1 monoclonal antibody (Invitrogen, Cat# MA5-23745, 8 mg/kg body weight)), anti-Ly6G (InVivoMab anti-mouse Ly6G, BioXcell Cat#BE0075-1, 500 µg/mouse), anti-NK1.1 (InVivoPlus anti-mouse NK1.1, BioXcell Cat#BP0036, 100 µg/mouse), GSK484 (GLPBI0, Cat#GC19184, 4 mg/kg body weight), anti-CD8 (InVivoPlus anti-mouse CD8α, Bioxcell Cat#BP0061, 100 µg/mouse), and IgG control (InVivoMab rat IgG1 isotype control, BioXcell Cat#BE0088, 10 mg/kg body weight) were used. These antibodies were administered intraperitoneally in the murine models. The mice were administered the anti-IgG thrice weekly over a period of 4 weeks. The anti-CXCL1, anti-Ly6G, anti-NK1.1, and anti-CD8 antibodies were administered twice weekly for a duration of 4 weeks.

All animal experiments were conducted in accordance with the approved protocols of the Institutional Animal Care and Use Committee (IACUC) at Sun Yat-sen University, and the approval number for this study is SYSU-IACUC-2021-000407. Animals were housed under specific pathogen-free conditions, maintained on a 12-hour light/dark cycle, and provided ad libitum access to food and water throughout the study.

Tissue collection from patients with ESCC

ESCC tissues were collected from patients who underwent surgical procedures at the First Affiliated Hospital, Sun Yat-Sen University. Tissue microarrays containing ESCC samples were obtained from the Sun Yat-sen University Cancer Center.

H&E staining

H&E staining was performed according to the manufacturer's instructions (Solarbio, G1120). Briefly, paraffin-embedded tissue sections were deparaffinized in xylene and rehydrated in a series of graded ethanol solutions. The sections were then stained with hematoxylin for 5 min, followed by differentiation in acid alcohol and bluing in running tap water. After that, the sections were counterstained with eosin for 2 min, dehydrated in ethanol, cleared in xylene, and mounted with a coverslip using mounting medium.

Immunohistochemistry

For IHC staining, the sections underwent antigen retrieval by heating in sodium citrate buffer (Bioss, C02-02002). Endogenous peroxidase activity was blocked with 3% hydrogen peroxide in methanol. Subsequently, the sections were washed with phosphate-buffered saline (PBS) three times and blocked with 5% bovine serum albumin (BSA) at 37°C for 1 hour to reduce non-specific binding. Next, the sections were incubated with primary antibodies at 4°C overnight. The primary antibodies used in this study included Ki67 (1:200, Novus, Cat#NB500-170), Cleaved Caspase-3 (1:200, CST, Cat#9661S), CD8a (1:500, Abcam, Cat#ab93278), CXCL1 (1:500, Proteintech, Cat#12335-1-AP), NCR1 (1:200, Abcam, Cat#ab283517), CD4 (1:300, Immunoway, Cat#YT0762), PI3k (1:200, Affinity, Cat#AF5112), and AKT (1:200, Proteintech, Cat#66444-1-Ig). The appropriate secondary antibodies were applied, followed by incubation with streptavidin–biotin complex (SABC) using the SABC immunohistochemical kit (BOSTER, Cat#SA1022). Subsequently, the sections were subjected to DAB staining (BOSTER, Cat#AR1027) to visualize the specific antigen–antibody complexes. To quantify the IHC staining results on patients with ESCC, the IHC staining intensity was assigned scores: 0 (negative), 1 (weak), 2 (medium), or 3 (strong), and IHC score was calculated by multiplying the percentage of positive cells (P) by the intensity (I), using the formula: $Q = P \times I$; with a maximum score of 300.³⁶ The IHC score was calculated based on the percentage of positive cells within ESCC mouse model.

Immunofluorescence

Paraffin-embedded tissue sections were subjected to antigen retrieval by heating in sodium citrate buffer. Endogenous peroxidase activity was quenched by treating the sections with 3% hydrogen peroxide in methanol. To reduce non-specific binding, sections were blocked with a fluorescent blocking solution (containing 1% BSA, 5% donkey serum, and 0.2% Triton X-100) at room temperature for 30 min. Subsequently, sections were incubated with primary antibodies overnight at 4°C. The primary antibodies used in this study included MPO (1:200, Immunoway, Cat#YM6663) and H3cit (1:200, Abcam, Cat#ab5103). Fluorescent secondary antibodies, conjugated with fluorochromes such as 488 and 594, were applied to the sections and incubated at room temperature for 50 min. After the incubation with secondary antibodies, sections were counterstained with DAPI (4',6-diamidino-2-phenylindole) to visualize cell nuclei and provide contrast.

scRNA-seq dataset analysis

scRNA-seq was performed on ESCC tissues obtained from epithelial conditional knockout CD276 (*K14^{CreER}, Cd276^{fllox/fllox}*) mice and control mice (*Cd276^{wt/wt}*) to elucidate the main mechanism by which CD276 regulates immune escape in ESCC. To prepare the single-cell suspension, esophageal tissues were microdissected and disaggregated into single cells using enzymatic digestion with mouse Tumor Dissociation Kit (130-096-730, Macs Miltenyi Biotec, China) at 37°C for 45 min using gentleMACS Dissociator (130-093-235, Macs Miltenyi Biotec, China). For scRNA-seq library preparation, we used the Chromium Single Cell 3' v3 (10× Genomics, Pleasanton, California, USA) following the manufacturer's instructions.

Seurat R package was employed to analyze and visualize the scRNA-seq data.³⁷ Briefly, we identified high-variable genes, capturing heterogeneity and key regulatory factors. Next, principal component analysis reduced dimensionality, enabling visualization of cellular heterogeneity, and identifying cell clusters based on gene expression patterns.

Comparative analysis between human and mouse ESCC models

Comparative analysis between human and mouse ESCC models was conducted using our scRNA-seq data and data from GSE160269.²³ To ensure comparability, orthologous genes between mouse and human datasets were identified. The cells from both datasets were integrated using Seurat's *sctransform* function, focusing on the most variable genes. The integrated cell matrix was generated using the *RunFastMNN* function (SeuratWrappers, V.0.1.0). Clustering and cell-type identification were performed using the Seurat package on the integrated dataset. The Sankey diagram visualized the origin of each cell type, enabling a comprehensive comparison of mouse and human ESCC cell types at the single-cell and whole transcriptome levels.

CellChat analysis

To explore and visualize the intricate communication networks between the tumor cell cluster and immune clusters, CellChat (version v1.1.0, github.com/sqjin/CellChat) was used.²⁴ Default parameter values were applied for each step of the analysis.

RNA-seq analysis

RNA-seq was conducted on ESCC tissues derived from epithelial conditional knockout CD276 mice and control mice. Briefly, total RNA was isolated using FreeZol reagent (Vazyme, Cat#R711-02) in accordance with the manufacturer's procedures. Then, total RNA was qualified and quantified using a NanoDrop and Agilent 2100 Bioanalyzer. The RNA library preparation was conducted using the MGISEQ500 platform (MGI Technology, MGISEQ-500). The gene count matrix was generated through alignment with the GRCm38 mouse reference genome. For RNA-seq analysis, the DEGs were identified by using DESeq2 (V.1.28.1) package in R.

Tissue dissociation and FCM analysis

To assess the immune cell population, we performed a comprehensive analysis of esophageal tissues from each group of mice (CD276 conditional knockout, CD276 conditional knock-in, and wild-type mice) following tamoxifen induction. The tissue dissociation process involved cutting the tissues into 2 mm pieces and successive rinses with prechilled PBS containing 3%, 5%, and 10% triple antibodies. Subsequently, tumor tissues were dissociated using the Metani Tumor Dissociation Kit (Miltenyi, 130-096-730) as per the manufacturer's instructions. The digested samples were then filtered and centrifuged at 1500 rpm for 5 min. Following the removal of the supernatant, erythrocyte lysis solution was added to lyse erythrocytes for 3 min. The lysis was terminated with PBS, and the cells were resuspended in 2% FBS to achieve a cell concentration of approximately 1×10^7 cells/mL. The samples were incubated on ice for 30 min and subsequently washed with PBS before centrifugation. For further immune cell characterization, the flow cytometric antibodies CD45 (1:50, Tonbo Biosciences, Cat#60-0451), CD3 (1:100, Tonbo Biosciences, Cat#20-0032), CD8a (1:100, Tonbo Biosciences, Cat#75-0081), CD4 (1:100, Biolegend, Cat#100510), GZMB (1:100, Biolegend, Cat#372212), CD25 (1:100, Tonbo Biosciences, Cat#50-0251), FOXP3 (1:100, Tonbo Biosciences, Cat#55-5773), CD11b (1:100, Tonbo Biosciences, Cat#85-0112), Ly6G (1:100, Tonbo Biosciences, Cat#50-1276), F4/80 (1:100, Invitrogen, Cat#45-4801-80), and NK1.1 (1:100, Tonbo Biosciences, Cat#80-5941) were incubated with the samples, following the same procedure as in the previous step. Finally, the samples were analyzed using an FCM analyzer to quantitatively and qualitatively assess the immune cell populations present in the esophageal tissues of the different mouse groups.

Statistical analyses

All experiments were independently repeated three times, and the data were presented as mean \pm SD to account for

experimental variability. GraphPad Prism V.8.0 software was used for statistical analysis and data visualization. To determine the significance of observed differences, log-rank test, two-tailed unpaired Student's t-test, and one-way analysis of variance with Tukey's multiple comparison test were employed. Significance levels are: "n.s" represents not significant, * $p < 0.05$, ** $p < 0.01$, and *** $p < 0.001$.

Author affiliations

¹Center for Translational Medicine, Sun Yat-sen University First Affiliated Hospital, Guangzhou, Guangdong, China

²Department of Thoracic Oncology, Sun Yat-sen University Cancer Center, Guangzhou, Guangdong, China

³Department of Radiation Oncology, Sun Yat-sen University First Affiliated Hospital, Guangzhou, Guangdong, China

⁴Institute for Advanced Study, Shenzhen University, Shenzhen, Guangdong, China

⁵Department of Plastic and Reconstructive Surgery, Shanghai Ninth People's Hospital, Shanghai Jiao Tong University School of Medicine, Shanghai, China

Contributors QZ and DC conceived of, designed, and supervised the study; GX, ZC, DC, and QZ performed the experiments and wrote the manuscript; FP and QL collected the clinical samples; YL, SC, and MC contributed to the experiments; CZ and RL analyzed the scRNA-seq and TCGA datasets. QZ is responsible for the overall content as the guarantor.

Funding This study was supported by the National Natural Science Foundation of China (No 82103658, No 82173362, No 81872409, and No 82304069), the Shanghai Pujiang Program (No 2022PJD040), the Guangdong Basic and Applied Basic Research Foundation (2019A1515110110), Guangdong Municipal Science and Technology Bureau (No 2024B03J1384), and China Postdoctoral Science Foundation (2023M734003).

Competing interests None declared.

Patient consent for publication Consent obtained directly from patient(s).

Ethics approval This study has received approval from the Ethics Committee of the First Affiliated Hospital, Sun Yat-sen University (B2021-131-01). Participants gave informed consent to participate in the study before taking part.

Provenance and peer review Not commissioned; externally peer reviewed.

Data availability statement Data are available in a public, open access repository.

Supplemental material This content has been supplied by the author(s). It has not been vetted by BMJ Publishing Group Limited (BMJ) and may not have been peer-reviewed. Any opinions or recommendations discussed are solely those of the author(s) and are not endorsed by BMJ. BMJ disclaims all liability and responsibility arising from any reliance placed on the content. Where the content includes any translated material, BMJ does not warrant the accuracy and reliability of the translations (including but not limited to local regulations, clinical guidelines, terminology, drug names and drug dosages), and is not responsible for any error and/or omissions arising from translation and adaptation or otherwise.

Open access This is an open access article distributed in accordance with the Creative Commons Attribution Non Commercial (CC BY-NC 4.0) license, which permits others to distribute, remix, adapt, build upon this work non-commercially, and license their derivative works on different terms, provided the original work is properly cited, appropriate credit is given, any changes made indicated, and the use is non-commercial. See <http://creativecommons.org/licenses/by-nc/4.0/>.

ORCID iDs

Demeng Chen <http://orcid.org/0000-0001-7230-2495>

Qimin Zhou <http://orcid.org/0000-0002-9480-4872>

REFERENCES

- Sung H, Ferlay J, Siegel RL, *et al*. Global cancer statistics 2020: GLOBOCAN estimates of incidence and mortality worldwide for 36 cancers in 185 countries. *CA Cancer J Clin* 2021;71:209–49.
- Smyth EC, Lagergren J, Fitzgerald RC, *et al*. Oesophageal cancer. *Nat Rev Dis Primers* 2017;3:17048.
- Ferlay J, Colombet M, Soerjomataram I, *et al*. Cancer statistics for the year 2020: an overview. *Int J Cancer* 2021.

- 4 Uhlenhopp DJ, Then EO, Sunkara T, *et al.* Epidemiology of esophageal cancer: update in global trends, etiology and risk factors. *Clin J Gastroenterol* 2020;13:1010–21.
- 5 Miyata H, Yoshioka A, Yamasaki M, *et al.* Tumor budding in tumor invasive front predicts prognosis and survival of patients with esophageal squamous cell carcinomas receiving neoadjuvant chemotherapy. *Cancer* 2009;115:3324–34.
- 6 Miller KD, Nogueira L, Mariotto AB, *et al.* Cancer treatment and survivorship statistics, 2019. *CA Cancer J Clin* 2019;69:363–85.
- 7 Kennedy LB, Salama AKS. A review of cancer immunotherapy toxicity. *CA Cancer J Clin* 2020;70:86–104.
- 8 Thompson JA. New NCCN guidelines: recognition and management of immunotherapy-related toxicity. *J Natl Compr Canc Netw* 2018;16:594–6.
- 9 Teixeira Farinha H, Digkila A, Schizas D, *et al.* Immunotherapy for esophageal cancer: state-of-the art in 2021. *Cancers* 2022;14:554.
- 10 Lu Z, Peng Z, Liu C, *et al.* Current status and future perspective of immunotherapy in gastrointestinal cancers. *Innovation (Camb)* 2020;1:100041.
- 11 Huang J, Xu J, Chen Y, *et al.* Camrelizumab versus investigator's choice of chemotherapy as second-line therapy for advanced or metastatic oesophageal squamous cell carcinoma (ESCORT): a Multicentre, randomised, open-label, phase 3 study. *Lancet Oncol* 2020;21:832–42.
- 12 Shen L, Kato K, Kim S-B, *et al.* RATIONALE 302: randomized, phase 3 study of Tislelizumab versus chemotherapy as second-line treatment for advanced Unresectable/metastatic Esophageal squamous cell carcinoma. *JCO* 2021;39:4012.
- 13 Sun J-M, Shen L, Shah MA, *et al.* Pembrolizumab plus chemotherapy versus chemotherapy alone for first-line treatment of advanced oesophageal cancer (KEYNOTE-590): a randomised, placebo-controlled, phase 3 study. *Lancet* 2021;398:759–71.
- 14 Doki Y, Ajani JA, Kato K, *et al.* Nivolumab combination therapy in advanced esophageal squamous-cell carcinoma. *N Engl J Med* 2022;386:449–62.
- 15 Kato K, Cho BC, Takahashi M, *et al.* Nivolumab versus chemotherapy in patients with advanced oesophageal squamous cell carcinoma refractory or intolerant to previous chemotherapy (ATTRACTION-3): a multicentre, randomised, open-label, phase 3 trial. *Lancet Oncol* 2019;20:1506–17.
- 16 Fukuoka S, Hara H, Takahashi N, *et al.* Regorafenib plus Nivolumab in patients with advanced gastric or colorectal cancer: an open-label, dose-escalation, and dose-expansion phase IB trial (REGONIVO, Epoc1603). *J Clin Oncol* 2020;38:2053–61.
- 17 Huang Y, Zhang H-L, Li Z-L, *et al.* Fut8-mediated aberrant N-Glycosylation of B7H3 suppresses the immune response in triple-negative breast cancer. *Nat Commun* 2021;12:2672.
- 18 Yonesaka K, Haratani K, Takamura S, *et al.* B7-H3 negatively modulates CTL-mediated cancer immunity. *Clin Cancer Res* 2018;24:2653–64.
- 19 Wang C, Li Y, Jia L, *et al.* Cd276 expression enables squamous cell carcinoma stem cells to evade immune surveillance. *Cell Stem Cell* 2021;28:1597–613.
- 20 Lee Y-H, Martin-Orozco N, Zheng P, *et al.* Inhibition of the B7-H3 immune checkpoint limits tumor growth by enhancing cytotoxic lymphocyte function. *Cell Res* 2017;27:1034–45.
- 21 Suh W-K, Gajewska BU, Okada H, *et al.* The B7 family member B7-H3 preferentially down-regulates T helper type 1-mediated immune responses. *Nat Immunol* 2003;4:899–906.
- 22 Prasad DVR, Nguyen T, Li Z, *et al.* Murine B7-H3 is a negative regulator of T cells. *J Immunol* 2004;173:2500–6.
- 23 Chen Y, Zhu S, Liu T, *et al.* Epithelial cells activate fibroblasts to promote esophageal cancer development. *Cancer Cell* 2023;41:903–18.
- 24 Jin S, Guerrero-Juarez CF, Zhang L, *et al.* Inference and analysis of cell-cell communication using cellchat. *Nat Commun* 2021;12:1088.
- 25 Teixeira Á, Garasa S, Gato M, *et al.* CXCR1 and CXCR2 Chemokine receptor agonists produced by tumors induce neutrophil extracellular traps that interfere with immune cytotoxicity. *Immunity* 2020;52:856–71.
- 26 Alfaro C, Teixeira A, Oñate C, *et al.* Tumor-produced Interleukin-8 attracts human myeloid-derived suppressor cells and elicits extrusion of neutrophil extracellular traps (nets). *Clin Cancer Res* 2016;22:3924–36.
- 27 Nie M, Yang L, Bi X, *et al.* Neutrophil extracellular traps induced by I18 promote diffuse large B-cell lymphoma progression via the TLR9 signaling. *Clin Cancer Res* 2019;25:1867–79.
- 28 Teixeira A, Garasa S, Ochoa MC, *et al.* I18, neutrophils, and nets in a collusion against cancer immunity and immunotherapy. *Clin Cancer Res* 2021;27:2383–93.
- 29 Haslam A, Prasad V. Estimation of the percentage of US patients with cancer who are eligible for and respond to checkpoint inhibitor immunotherapy drugs. *JAMA Netw Open* 2019;2:e192535.
- 30 Leitner J, Klausner C, Pickl WF, *et al.* B7-H3 is a potent inhibitor of human T-cell activation: no evidence for B7-H3 and TREM2 interaction. *Eur J Immunol* 2009;39:1754–64.
- 31 Veenstra RG, Flynn R, Kreyborg K, *et al.* B7-H3 expression in donor T cells and host cells negatively regulates acute graft-versus-host disease lethality. *Blood* 2015;125:3335–46.
- 32 Chen X, Quinn EM, Ni H, *et al.* B7-H3 participates in the development of experimental pneumococcal meningitis by augmentation of the inflammatory response via a Tlr2-dependent mechanism. *J Immunol* 2012;189:347–55.
- 33 Picarda E, Ohaegbulam KC, Zang X. Molecular pathways: targeting B7-H3 (Cd276) for human cancer immunotherapy. *Clin Cancer Res* 2016;22:3425–31.
- 34 Du H, Hirabayashi K, Ahn S, *et al.* Antitumor responses in the absence of toxicity in solid tumors by targeting B7-H3 via chimeric antigen receptor T cells. *Cancer Cell* 2019;35:221–37.
- 35 Seaman S, Zhu Z, Saha S, *et al.* Eradication of tumors through simultaneous ablation of CD276/B7-H3-positive tumor cells and tumor vasculature. *Cancer Cell* 2017;31:501–15.
- 36 Wang X, Li K, Cheng M, *et al.* Bmi1 severs as a potential tumor-initiating cell marker and therapeutic target in esophageal squamous cell carcinoma. *Stem Cells Int* 2020;2020:8877577.
- 37 Hao Y, Hao S, Andersen-Nissen E, *et al.* Integrated analysis of multimodal single-cell data. *Cell* 2021;184:3573–87.